Full Paper

Journal of Agricultural Meteorology 71 (1): 32-50, 2015

Special Collection: Sensing and Monitoring Research Group, SAMJ

FluxPro as a realtime monitoring and surveilling system for eddy covariance flux measurement

Wonsik KIM [a,†], Akira MIYATA [a], Ali ASHRAF [b], Atsushi MARUYAMA [c], Amnat CHIDTHAISONG [d], Chaiporn JAIKAEO [e], Daisuke KOMORI [f], Eiji IKOMA [g], Gen SAKURAI [a], Hyeong-Ho SEOH [h], In Chang SON [i], Jaeil CHO [j], Jonghyeon KIM [k], Keisuke ONO [a], Korakod NUSIT [l], Kyung Hwan MOON [i], Masayoshi MANO [m], Masayuki YOKOZAWA [n], Md. Abdul BATEN [b], Montri SANWANGSRI [o], Motomu TODA [p], Nittaya CHAUN [d], Panya POLSAN [q], Seiichiro YONEMURA [a], Seong-Deog KIM [r], Shin MIYAZAKI [s], Shinjiro KANAE [t], Suban PHONKASI [l], Sukanya KAMMALES [d], Takahiro TAKIMOTO [a], Taro NAKAI [u], Toshichika IIZUMI [a], Vanisa SURAPIPITH [v], Warangluck SONKLIN [l], Yong LEE [w], Yoshio INOUE [a], Youngwook KIM [x], and Taikan OKI [g]

[a] National Institute for Agro-Environmental Sciences 3-1-3 Kannondai, Tsukuba, Ibaraki, Japan
[b] Bangladesh Agricultural University, Mymensingh, Bangladesh
[c] National Agriculture and Food Research Organisation, 3-1-1 Kannondai, Tsukuba, Ibaraki, Japan
[d] Joint Graduate School of Energy and Environment, King Mongkut's University of Technology Thonburi, and Center for Energy Technology and Environment, Ministry of Education, Bangkok, Thailand
[e] Kasetsart University, 50 Ngam Wong Wan Road, Ladyaow Chatuchak, Bangkok, Thailand
[f] Tohoku University, 6-6-06 Aoba, Aramaki, Aoba-ku, Sendai, Japan
[g] Institute of Industrial Science, The University of Tokyo, 4-6-1 Komaba Meguro-ku, Tokyo, Japan
[h] National Institute of Horticultural and Herbal Science, Cheoncheon-ro, Jangan-gu, Suwon, Gyeonggi-do, Korea
[i] Agricultural Research Center for Climate Change, 316 Ayeonno, Jeju, Korea
[j] Korea Research Institute for Human Settlements, 254 Simindae-ro, Dongan-gu, Anyang-si, Gyeonggi-do, Korea
[k] Soldan Incorporated, B-610, Garden5-works, Chungmin-ro 52, Songpa, Seoul, Korea
[l] Naresuan University, 99 Moo 9 Tambon Thapho, Muang, Thailand
[m] Chiba University, 1-33, Yayoi-cho, Inage-ku, Chiba-shi, Chiba, Japan
[n] Shizuoka University, 3-5-1 Johoku, Naka-ku, Hamamatsu, Japan
[o] University of Phayao, 19 Moo 2, Phahonyothin Rd, Tambon Maeka, Amphur Muang, Phayao, Thailand
[p] Hiroshima university, 1-7-1 Kagamiyama, Higashi-Hiroshima, Japan
[q] Royal Irrigation Department, 811 Samsen, Nakornchaisri, Dusit, Bangkok, Thailand
[r] Chungnam National University, 99, Daehak-ro, Yuseong-gu, Daejeon, Korea
[s] Japan Agency for Marine-Earth Science and Technology, 3173-25 Showa-machi, Kanazawa-ku, Yokohama-city, Kanagawa, Japan and National Institute of Polar Research, 10-3, Midori-cho, Tachikawa-shi, Tokyo, Japan
[t] Tokyo Institute of Technology, 2-12-1 O-okayama, Meguro-ku, Tokyo, Japan
[u] Nagoya University, Furo-cho, Chikusa-ku, Nagoya, Japan
[v] Pollution Control Department, 404 Phaholyothin Rd., Samsen Nai, Phayathai, Bangkok, Thailand
[w] WeatherTech, 1587-17 Sillim1-dong, Gwanak-gu, Seoul, Korea
[x] Numerical Terradynamics Simulation Group, The University of Montana, Missoula, MT 59812, USA

Abstract

To understand how terrestrial ecosystems respond to global climate change, researchers have globally measured the energy, water and carbon dioxide flux densities (F) globally over various types of vegetation by the eddy covariance (EC) method. However, the process of F calculation and the method of quality control and quality assurance (QCQA) are complex and site specific. Moreover, instantly maintaining remote EC flux measurement sites against instrumentation problems and administrative difficulties is laborious. To overcome these issues, particularly those of realtime F monitoring and prompt site management, *FluxPro* was created.

FluxPro consists of three functional systems: 1) a gathering system that transports EC measurements from various sites to the *FluxPro* management server; 2) a cooking system that computes F and its frictional uncertainty (ε) together with micrometeorological variables (V); and 3) a serving system that presents the results of the gathering and cooking systems as charts to be distributed over the internet in realtime. Consequently, *FluxPro* could become an appropriate system for realtime-multi-site management, since it not only automatically monitors F with ε and V but also continuously surveils EC sites, including copious information and an email alert system.

Key words: Eddy covariance measurement, *FluxPro*, Frictional uncertainty, Realtime-multi-site management.

Received; July 18, 2014.
Accepted; October 3, 2014.
† Corresponding Author: wonsik@affrc.go.jp
DOI: 10.2480/agrmet.D-14-00034

1. Introduction

During the past few decades, the number of eddy covariance (EC) flux measurement sites, installed for measuring evapotranspiration (*E*) and carbon dioxide flux (F_c), has dramatically increased. Currently, over 500 such sites are distributed in ecosystems across the world (http://fluxnet.ornl.gov). Together with numerical simulations and satellite observations, EC measurements have assisted the colleagues to estimate the *E* and F_c exchanges between land surfaces and the atmosphere, and their fluctuations under global climate change, and vice versa (Baldocchi *et al*., 2001; Li *et al*., 2009; Lu *et al*., 2005; Jung *et al*., 2011; Kim *et al*., 2012). The outstanding contributions of EC measurement have been facilitated by the development of instruments and the integration of micrometeorological knowledge. Taking measurements in realtime will enable present estimations and predictions of *E* and F_c for the practical management of water and biomass resources over land surfaces.

Measurement is the process of determining the value of a physical quantity and its inaccuracy using customized experimental techniques and appropriate instruments (Rabinovich, 2005). EC measurements provide both the flux density (*F*) and its frictional uncertainty (ε); however, few studies have shown ε on the basis of hourly *F*. Meanwhile, ε is relevant in hybrid model-data fusion studies when measured data are limited, and methods for estimating the hourly ε have been already proposed (Finkelstein and Sims, 2001). In addition, ε provides the effective heterogeneity (Kim *et al*., 2011b), which is closely related to the Bowen ratio (Kim *et al*., 2014) representing land surface variability. Therefore, the realtime estimation of ε with *F* could be anticipated to contribute the diminishment of the data gap of flux monitoring and the improvement of the forecasting capability (Sheffield *et al*., 2014) through data assimilation (Kato *et al*., 2013).

Since the first attempt to construct a realtime monitoring and simulation system (RTMASS) for EC measurements (Kim *et al*., 2003), communication technology has improved to the extent that EC measurements can be relayed from remote sites to the RTMASS server, and more technical developments are expected. Using the estimation method recommended by Kim *et al*. (2009, 2011b), ε can be estimated for a quality control and quality assurance (QCQA) and a heterogeneity parameters in the EC measurements.

Considering the points so far, this study aims to introduce *FluxPro* as a convenient and appropriate utensil for monitoring *F* and surveilling sites of continuous realtime EC measurements, We also report findings obtained throughout the *FluxPro* operation.

2. The structure of *FluxPro*

FluxPro integrates three functional systems: 1) the gathering system (*G system*) acquires EC measurements from instruments installed at various remote sites; 2) the cooking system (*C system*) estimates *F* together with ε and several micrometeorological variables (*V*) using the measurements gathered by the *G system*; and 3) the serving system (*S system*) delivers the estimates computed by the *C system* over the internet in user-friendly formats.

2.1 *G system* for gathering EC measurements

The *G system* transports turbulence and micrometeorological time series from remote sensors installed at EC measurement sites to the *C system*. The *G system* consists of commercial hardware (measurement sensors and recordable loggers), and commercial and self-created software (telecommunication and telemonitoring applications).

2.1.1 Hardware instrumentation

The EC system of the *G system* includes a three-dimensional sonic anemometer (CSAT3: Campbell Scientific, Utah, USA; DA-600: Kaijo Corporation, Tokyo, Japan; R3-50: Gill Instruments, Hampshire, UK), an open-path CO_2/H_2O gas analyzer (LI7500: LI-COR, Nebraska, USA or EC150: Campbell Scientific), and a measurement and control datalogger (CR1000, CR3000 or CR5000: Campbell Scientific) optionally equipped

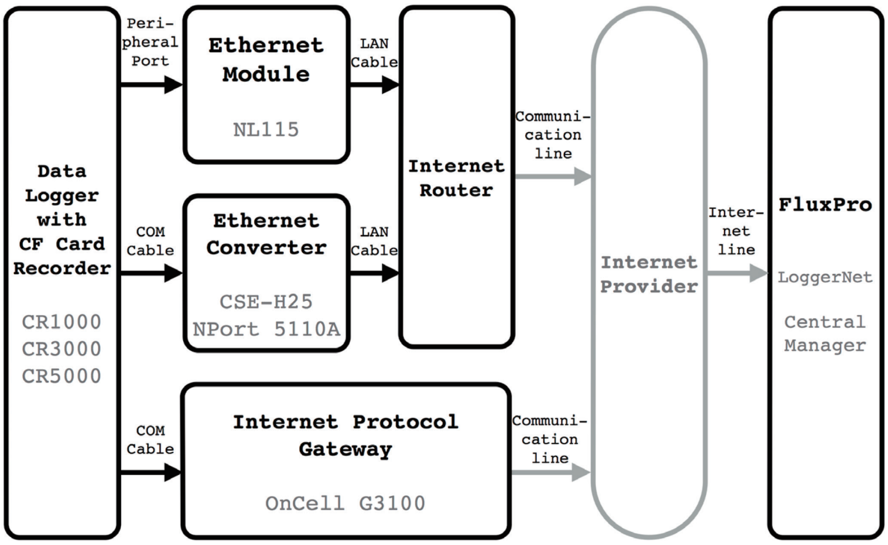

Fig. 1. Schematic of the three telecommunication routes in the gathering system. Boxes to the left and right of the gray arrows are local instruments and the *FluxPro* management server, respectively. The names or titles of devices are given in the bold font; the remaining text gives the name of the component. Black arrows denote a wired lines; gray arrows denote wired or wireless lines (CF: compact flash; COM: communication port; LAN: local area network).

with a compact flash (CF) module (CFM100 or NL115: Campbell Scientific). The anemometer and the analyzer are operated by a synchronous device for measurements (SDM), by which the turbulence time series of vectors, *i.e.*, the longitudinal (u), lateral (v) and vertical (w) wind velocities, and scalars, *i.e.*, the quantities (ξ) of temperature (T) and densities of CO_2 and H_2O (ρ_c and ρ_w, respectively) at atmospheric pressure (p) are sensed at 10 Hz and directly recorded into the CF card installed in the data logger module. The net radiometer (CNR4: Campbell Scientific) and weather transmitter (WXT510: Campbell Scientific) are operated by an analog signal. The micrometeorological time series, *i.e.*, the downward short- and long-wave radiation (R_s and R_l, respectively), the air temperature and vapor pressure (T_a and e_a, respectively), and precipitation (P) are also sensed at 10 s intervals, and the 10 min mean is recorded onto the CF card.

The *G system* offers three telecommunication routes, as shown in Fig. 1. The first uses the Ethernet module (NL115). By this route, the time series saved at a CF card installed in the module is transported to the *FluxPro* server through an internet router connected to a commercial internet service provider. The second uses the Ethernet converter (CSE-H25: Sollae Systems, Seoul, Korea or NPort 5110A: Moxa, Taipei, Taiwan) to connect with the communication port (COM) as an alternative transport route instead of NL115. The final route uses the internet protocol (IP) gateway (OnCell G3100: Moxa), without the router as equipped in a standardized virtual private cellular network.

2.1.2 Software configuration

The global IP address (GIP) is best distributed to each local Ethernet device by either the first or second route, as described in Subsection 2.1.1. However, GIP limitations may restrict this information dissemination in practice. Therefore, it is recommended that the device installed at each telecommunication site be configured with a dynamic domain name system (DDNS) served by an online provider free of charge. Suitable choices are both GIP and DDNS, the IPPort option of LoggerNet (Campbell Scientific), a telemonitoring application that runs on Windows (Microsoft, Seattle, USA). In the third telecommunication route, the OnCell Central Manager (Moxa) is additionally installed in Windows, enabling telecommunication with OnCell G3100 using the Reverse Real COM Mode. The mode requires that the GIP address be assigned to the *G system* of *FluxPro*'s management server, where the Central Manager is installed. By means of the created virtual COM port of the Central Manager, the ComPort option of LoggerNet is configured.

A time series of turbulence and micrometeorological measurements recorded in the CF card of each remote site is regularly transported to the *FluxPro* server and is temporarily stored in a home directory folder named *mdata* using LoggerNet, which runs only on Windows. The home directory folder is directly referred by several functions of *FluxPro* running on Darwin (Apple, Cupertino, California, USA), described below. Therefore, for ease of data management, Windows should be installed on Darwin with VMware Fusion (VMware, California, USA) or Parallels Desktop (Parallels, Washington, USA).

2.1.3 Primary database

An additional role of the *G system* is to construct a database of turbulence and meteorological measurements that are conveyed from each of the remote sites. The measurements temporally stored in *mdata* are moved to two home directory folders named *odata* and *rdata*. The *odata* folder stores the original data for one day for backup purposes only, while *rdata* stores the raw data for one hour to enable the F computation. Although the measured contents of *odata* and *mdata* are identical, *rdata* is converted to a UNIX file containing a time tag, u, v, w, T, ρ_c, ρ_w and p only, which are separated by a space separator. Both data set are physically placed in a storage configured RAID (redundant array of independent disks) 5 in the *FluxPro* server and are mirrored to a server located in another room for security backup purposes. The *odata* and *rdata* datasets can also be mirrored to the local server, which is managed by the principal investigator (PI). Local servers retain their own data sets of measurements collected from individual flux sites. In addition, the *FluxPro* can automatically send an alert email to the PI to check daily the content of the turbulence time series relayed from each site.

2.2 *C system* for cooking EC estimates

The F computation described in Kim *et al*. (2011b, a) is a fundamental function of *FluxPro* and is processed by the *C system*. Operating on Darwin, *FluxPro* is written in Bash (Bourne Again SHell, http://www.gnu.org/software/bash/) and GFortran (GNU Formula Translating System, http: //gcc.gnu.org/fortran/), both computing languages created by GNU (http://www. gnu.org). *FluxPro*, it contains three process procedures: 1) initial inspection of turbulence measurements to examine the availability of time series; 2) main computation of F and ε to estimate F and secure its credibility; and 3) supplementary calculation of V to validate the quality of F (namely, ε), and to describe the circumstances under which F is estimated.

2.2.1 Initial inspection

The inspection of a turbulence time series is carried out in the six following steps, yet some steps for fundamental corrections are omitted to guarantee a communal system required by *FluxPro*.

1) Spike correction: Vickers and Mahrt (1997) suggested that spiking events are limited to three or fewer consecutive points, and that three times of the standard deviation (σ) is a suitable threshold for spike detection in the turbulence time series. They replaced the spikes with interpolation between before and after the spike, imposing a 1% criterion on the tolerated number of spikes. In *FluxPro*, however, the spiking threshold is 5σ, and the spike is substituted by the mean of the time series to minimize measurement rejection by the threshold and the effect of the infill values on F.

2) Tilt correction: Finnigan (2004) recommended the planar-fit method for the coordinated transformation, *FluxPro* employs the double rotation method (Kaimal and Finnigan, 1994) because the estimation of planar-fit coefficients is insufficient for realtime monitoring.

3) Trend correction: The detrending of a time series is not performed in *FluxPro*.

4) Frequency correction: The high frequency correction is not performed in *FluxPro* because the classical spectral model is applicable only to low-lying vegetation in homogeneous environments (Massman and Clement, 2004), whereas *FluxPro* demands wide applicability.

5) Crosswind correction: No crosswind correction (Liu *et al*.,

2001) is required because CSAT3 and R3-50 correct online for the effect of wind blowing perpendicular to the sonic path with the exception of DA-600.

6) Humidity correction: The correction to sonic virtual temperature is traditionally carried out in accordance with Kaimal and Gaynor (1991).

2.2.2 Main computation

The main computation to estimate F and ε including additional corrections is conducted according to the following five steps.

1) The F computation: Kim *et al.* (2011b) found that the lowest uncertainty appeared when the turbulence measurements were estimated over 1 hour to 5 hours, and that an hourly estimate captured the highest temporal resolution. Therefore, the F given by *FluxPro* is estimated over intervals of 1 hour. This setting approximately accords with findings of Finnigan *et al.* (2003) and Moncrieff *et al.* (2004). Using the 1 hour turbulence time series of w and ξ, F is computed by the EC method as follows:

$$F = \overline{w'\xi'}, \tag{1}$$

where

$$\overline{w'\xi'} = \frac{1}{N}\sum_{t=0}^{N-1}(w_t - \overline{w})(\xi_t - \overline{\xi}), \tag{2}$$

N is set to 36000 and t is the time index. The $^-$ and $'$ embellishments denote a mean and deviation operator, respectively.

2) The ε computation: The fractional uncertainty ε, which quantifies the uncertainty in the hourly F, is defined as

$$\varepsilon = \frac{\sigma_{w\xi}}{|F|} \tag{3}$$

(Kim *et al.*, 2011b), where

$$\sigma_{w\xi} = \sqrt{\frac{1}{N}\left(\sum_{h=-m}^{m}\gamma_{ww}(h)\gamma_{\xi\xi}(h) + \sum_{h=-m}^{m}\gamma_{w\xi}(h)\gamma_{\xi w}(h)\right)} \tag{4}$$

(Meyers *et al.*, 1998; Finkelstein and Sims, 2001). In Equation (4), m is the number of samples that are sufficiently large to capture an integral timescale (set to 200 in our calculation) and autocovariance of the lag time h is given by

$$\gamma_{\xi\xi}(h) = \gamma_{\xi\xi}(-h) = \frac{1}{N}\sum_{t=1}^{N-h}(\xi_t - \overline{\xi})(\xi_{t+h} - \overline{\xi}). \tag{5}$$

The cross-covariance of the lag time h is given by

$$\gamma_{w\xi}(h) = \gamma_{\xi w}(-h) = \frac{1}{N}\sum_{t=1}^{N-h}(w_t - \overline{w})(\xi_{t+h} - \overline{\xi}). \tag{6}$$

In *FluxPro*, ε was considered to merit the QCQA parameter because it depends on both spatial and temporal scales according to various supporting studies (Kim *et al.*, 2009, 2011a,b, 2014).

3) Density correction: The corrections to lE are conducted as described in Webb *et al.* (1980) and Leuning (2004) after ε has been estimated.

4) Heating correction: The influence of instrument surface heat exchange on the estimation of F using LI7500 (Burba *et al.*, 2008) is not now considered in *FluxPro*. However, we are requesting colleagues to correct this factor to improve *FluxPro*.

5) Data integration: Gap filling is regarded as a crucial process in integrating EC measurements, and various methods have been suggested (Falge *et al.*, 2001). *FluxPro* integrates the yearly F as

$$F_{\text{year}} = \sum_{i=1}^{12}\sum_{k=0}^{23} JF_{ik}, \tag{7}$$

using a weighted mean diurnal variation such as

$$F_{ik} = \frac{\sum_{j=1}^{J}\frac{F_{ijk}}{\varepsilon_{ijk}^2}}{\sum_{j=1}^{J}\frac{1}{\varepsilon_{ijk}^2}}, \tag{8}$$

where J is one of 28, 29, 30 or 31 depending on the month, and i, j and k are indexes denoting the month, day and hour, respectively. The σ of the weighted mean of the uncertainty of F_{year} is defined as

$$\sigma_{\text{year}} = \sum_{i=1}^{12}\sum_{k=0}^{23} J\sigma_{ik}, \tag{9}$$

where

$$\sigma_{ik} = \frac{\sum_{j=1}^{J}\frac{(F_{ijk} - \overline{F}_{ik})^2}{\varepsilon_{ijk}^2}}{\sum_{j=1}^{J}\frac{1}{\varepsilon_{ijk}^2}}. \tag{10}$$

This method is an additional improvement in making estimates of the annual integration when F gap is continuously longer than a couple of weeks, so we are developing a numerical model to fill the gaps with its output.

2.2.3 Supplementary calculation

FluxPro provides several customary supplementary V to confirm the effect of a circumstance on F and the confidence of the F measurements. The estimated Vs are described below:

1) Friction velocity:

$$u_* = \sqrt[4]{(\overline{u'w'})^2 + (\overline{v'w'})^2}, \tag{11}$$

The u_* is traditionally applied to understand turbulence intensity in the measured F. Several studies adopted u_* as the QCQA parameter of EC measurements. However, *FluxPro* uses ε instead of u_*, since the uncertainty information contained in ε is more suitable for quality estimation than for a correction threshold.

2) Integral turbulence characteristics:

$$\phi_\xi = \frac{\sigma_\xi}{|\xi_*|}, \tag{12}$$

where

$$\sigma_\xi = \sqrt{\overline{\xi'^2}}, \tag{13}$$

$$\xi_* = -\frac{\overline{w'\xi'}}{u_*}. \tag{14}$$

The ϕ is the ratio of the standard deviation of a turbulence parameter to the turbulence flux. It is comparable to the atmospheric stability function known as the Monin-Obukhov similarity, which describes developed turbulence conditions (Kaimal and Finnigan, 1994; Foken and Wichura, 1996), while constant parameters remain contentious.

3) The atmospheric stability:

$$\zeta = \frac{z}{L}, \tag{15}$$

where z is the height above the zero-plane displacement, and L is the Monin-Obukhov length, defined as

$$L = -gk\frac{\overline{w'\theta'}}{u_*^3\overline{\theta}}, \tag{16}$$

with potential temperature

$$\theta = T + 273.15 + \frac{g}{c_\mathrm{p}}\Delta z, \tag{17}$$

In Equation (17), g, c_p and Δz represent the acceleration due to gravity, the specific heat at constant p, and the height difference relative the 100 kP level, respectively.

4) Correlation coefficient:

$$r_{w\xi} = \frac{\overline{w'\xi'}}{\sigma_w\sigma_\xi}, \tag{18}$$

It is also presented in *FluxPro*.

2.2.4 EC database

The F, together with ε and V, is computed every hour (Table 1). The results of each site are saved in the *edata* folder within the home directory. The *edata* is publicly linked to the *FluxPro* webpage (*e.g.* http://matthew.niaes.affrc.go.jp/amen/fluxpro/annual_ctt007.html) at the discretion of the site PI. However, a *edata* which is not allowed open in public by the PI posted to the PI alone, overrides the *FluxPro*'s policy that data be made publicly available.

2.3 *S system* for serving over internet

Various F and V charts monitored by the *G system* and computed by the *C system* are scripted in HTML (http://www.w3.org/html/) and Bash including the GMT (Generic Mapping Tools, http://gmt.soest.hawaii.edu) commands and ImageMagick (http://www.imagemagick.org) for the *FluxPro* webpage. Each cart is linked to four tabs (*i.e. flux*, *raw*, *meteo* and *annual*), visible in the left frame of the *FluxPro* on *AgroMeteorological Nowcaster* webpage (http://matthew.niaes.affrc.go.jp/amen/), and is renewed on an hourly basis.

2.3.1 The *flux*: Fundamental analysis of F and ε

Table 1. File formats of the EC database of *FluxPro*.

Column	Variables	Abbreviation	Unit
01	Timetag (day of year and hour of day)	doyhh	
02	Sensible heat flux	H	W m^{-2}
03	Fractional uncertainty of H	ε_H	dimensionless
04	Latent heat flux	lE	W m^{-2}
05	Fractional uncertainty of lE	ε_{lE}	dimensionless
06	Carbon dioxide flux	F_c	mg m^{-2} s^{-1}
07	Fractional uncertainty of F_c	ε_{Fc}	dimensionless
08-09	NF		
10	Wind direction	W_d	°
11	Atmospheric stability	ζ	dimensionless
12	Frictional velocity	u_*	m s^{-1}
13	Variability in w	ϕ_w	dimensionless
14	Variability in θ	ϕ_θ	dimensionless
15	Variability in ρ_c	$\phi_{\rho c}$	dimensionless
16	Variability in ρ_w	$\phi_{\rho w}$	dimensionless
17	Correlation coefficient between u and w	r_{uw}	dimensionless
18	Correlation coefficient between w and θ	$r_{w\theta}$	dimensionless
19	Correlation coefficient between w and ρ_w	$r_{w\rho w}$	dimensionless
20	Correlation coefficient between w and ρ_c	$r_{w\rho c}$	dimensionless
21-25	NF		
26	Mean of u	μ_u	m s^{-1}
27	Standard deviation of u	σ_u	m s^{-1}
28	Mean of v	μ_v	m s^{-1}
29	Standard deviation of v	σ_v	m s^{-1}
30	Mean of w	μ_w	m s^{-1}
31	Standard deviation of w	σ_w	m s^{-1}
32	Mean of T	μ_T	℃
33	Standard deviation of T	σ_T	℃
34	Mean of ρ_c	$\mu_{\rho c}$	mg m^{-3}
35	Standard deviation of ρ_c	$\sigma_{\rho c}$	mg m^{-3}
36	Mean of$\phi\rho_w$	$\mu_{\rho w}$	g m^{-3}
37	Standard deviation of ρ_w	$\sigma_{\rho w}$	g m^{-3}
38-41	NF		

The meanings of the turbulence time series, *i.e.* u, v, w, T, ρ_c and ρ_w are provided in Subsection (2.1.1); NF: Not fixed.

Five representative charts of F and ε together with traditional QCQA parameters are analyzed under the *S system* tab *flux* on the *FluxPro* webpage (Table 2 and Figs. 2–6).

1) The *week* chart (Fig. 2) presents the F trends of sensible and latent heat fluxes (H and lE, respectively) and F_c over one week, together with V trends of W_d, ζ and u_*. The whiskers written in F trends denote $\pm 1\sigma$ as an absolute uncertainty Both F and V trends are colored according to the scale of ε and Taylor's parameter τ, respectively. The τ is given by

$$\tau = \frac{2\sigma_M}{M}, \tag{19}$$

where,

$$M = \sqrt{u^2 + v^2}. \tag{20}$$

The range in the F trend, namely $\varepsilon \pm 3\sigma_\varepsilon$, is stated in the left-upper region of each subchart. The range is calculated from the hourly fluctuations in Fig. 3. Assuming Taylor's Hypothesis (Willis and Deardorff, 1976; Stull, 1988), the τ is fixed (between 0.6 and 1.4) over the range in the V trend, indicating that the eddy scarcely changes as it advects past the sensor. This situation satisfies the measurement assumption in the EC method; namely, that the flow is not distorted by obstacles or an insufficient fetch length. The vertical gray region denotes where turbulence measurements were missing or rejected as out of range (lE or $H < -300$ or lE or $H >$ 1000 W m^{-2}, $F_c < -4.0$ or $F_c > 1.5$ mg m^{-2} s^{-1}, $\sigma_{lE,H} > 70$ Wm^{-2}, $\sigma_{Fc} > 0.28$ mg m^{-2} s^{-1}, and $\varepsilon > 1.0$) even in regions of acceptable turbulence computations. The two numerals in the right-upper side of each subchart of Fig. 2 denote the F acquisition ratio over one week within the specified ε range. The upper numeral specifies the total F ratio (obtained by summing all circles); the lower numeral (in color) sums only the measured fluxes within the ε range (colored circus in the subplots).

2) The chart named *epsilon* (Fig. 3) plots the relationship between ε and F (scaled by ζ) in each bin of the ε histogram. The dotted line and grey region indicate the median ε and its 1σ deviation, respectively, over the week-long period. Kim *et al.* (2011a) defined an expected value of ε called the tolerance (see Equation (2)), which combines the random uncertainty δ_r ($\simeq$0.07, dashed line Fig.3) with an illegitimate uncertainty δ_i. The δ_r is similar to white noise and is therefore considered constant, while δ_i irregular and produced by deviations from an illegitimacy of the EC measurement assumption. The numerals in the bottom-right corner of sub charts specify the weekly $\varepsilon \pm \sigma$, and whereas those in the top-right corner of the insets (displaying the histograms) specify the kurtosis (upper) and skewness (lower).

3) The *sigma* chart (Fig. 4) plots the relationship between σ and F (scaled by ζ) over one week. The subcharts in the right column are enlargements of the regions delineated by rectangles in the corresponding left subcharts. The diagonals in the right subchart denote the line of 1.00 by 0.07 decided by δ_r described in the previous section. The relationship between σ and F is clearly linear at H. Such a linear relationship has been previously reported by Finkelstein and Sims (2001), Hollinger and Richardson (2005), Vickers *et al.* (2009) and our group (Kim *et al*., 2008, 2009, 2011a,b). This information is significant not only for the QCQA of F but also for understanding the relationship between δ_r and δ_i in ε, where the distance from the diagonal line denotes the magnetite content of δ_i in δ. Interestingly, ε and u_* are unrelated (data not shown) and ε lower than 0.07 is existed (details are presented at Subsection 3.2).

4) The *variability* chart (Fig. 5) presents ϕ (refer to Subsection 2.2.3) and the correlation coefficient r against ζ (scaled by ε) over one week. The dashed and dotted lines (be specified to w and θ, respectively) within the graduated gray region (±15% deviation interval from the lines) denote the lines of

$$\phi_w = \begin{cases} 1.25(1+3.0|\zeta|)^{\frac{1}{3}}, & -2 \le \zeta \le 0 \\ 1.25(1+0.2\zeta), & 0 \le \zeta \le 1 \end{cases} \tag{21}$$

and

Table 2. List of charts in serving system of *FluxPro* (http://matthew.niaes.affrc.go.jpa/amen).

Tab	Chart	Figure	Program
flux	*week*	2	wfx2er
	epsilon	3	wto2fx
	sigma	4	sig2flx
		5	wsf2zlt
	variability	-	phi2zlt
		-	wsf2zlu
	variation	6	mdvlhfcdf
		-	mdvshfcdf
raw	*series**	7	rdana
	*spectrum**	8	wfsfflux
meteo	*radiation*	9	wradi
	meteorology	10	wtrend
	EC	11	wrange
	windrose	12	windrose
annul	*trend***	13	annflux
	*contour***	14	hryrgrid

*24 panels (hourly data) are presented for one day; **Panels are presented for every measured year.

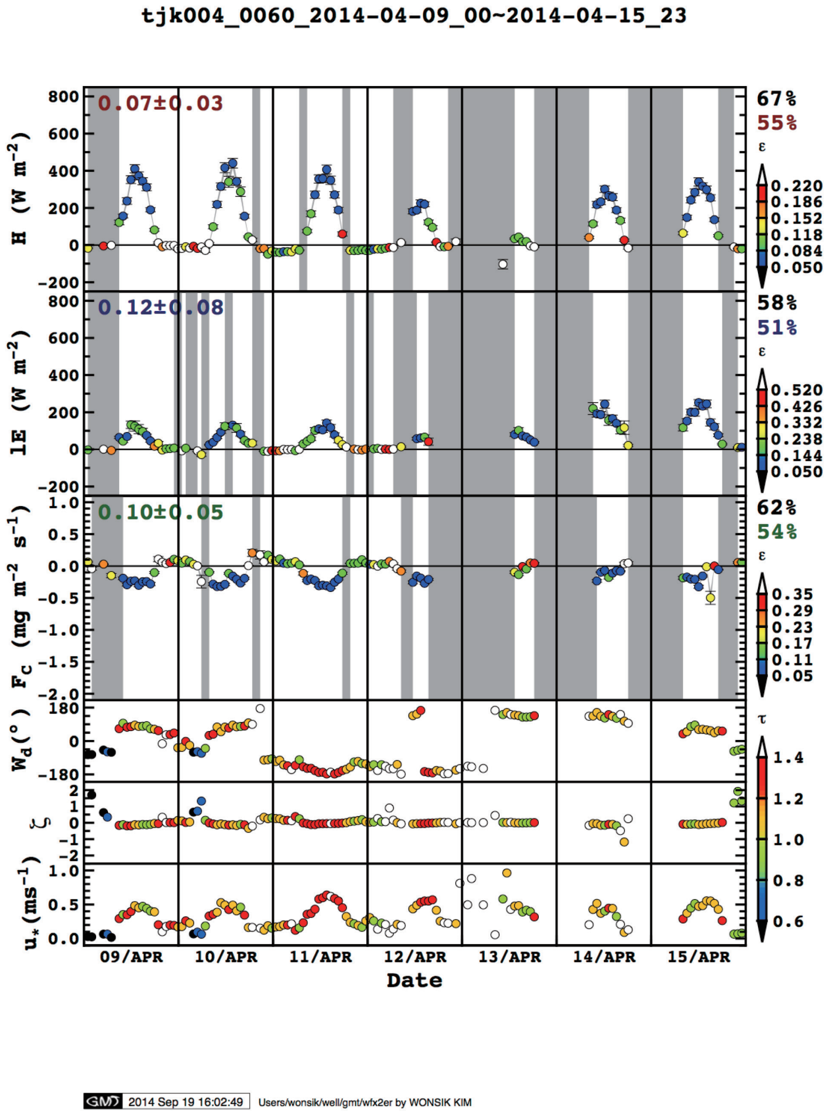

Fig. 2. The chart named *week* in the *flux* cluster of *FluxPro*, showing the temporal trends of H, lE and F_c with 1σ whiskers. Trends of W_d, ζ and u_* are also plotted. Turbulence measurements were taken from 00:00:00 0 Hz on 9 April to 23:59:59 9 Hz on 15 April, 2014 at a tangerine orchard in Jeju, Korea. Title (left to right) gives: site ID_block size (min) of estimated F_start year–start month–start day_start hour～end year–end month–end day_end hour. Details are given in 1) of Subsection 2.3.1.

$$\phi_\theta = \begin{cases} 2(1+9.5|\zeta|)^{-\frac{1}{3}}, & -2 \le \zeta \le 0 \\ 2(1+0.5\zeta)^{-1}, & 0 \le \zeta \le 1 \end{cases} \tag{22}$$

in the ϕ plots, and

$$r_{uw} \simeq -0.35, \quad -1 \le \zeta \le 1 \tag{23}$$

and

$$r_{w\theta} = \begin{cases} 0.5, & -2 < \zeta < 0 \\ 0, & \zeta = 0 \\ -0.4, & 0 < \zeta < 1 \end{cases} \tag{24}$$

in the r plot (Kaimal and Finnigan, 1994). By analyzing ϕ and r, we obtain significant information on the developed turbulence, since both parameters are sensitive to violated stationarity caused by limitations of the surface layer height, gravity waves, internal boundary layers, flow distortion, and loss of high frequency flux (Foken *et al*., 2004; Massman and Clement, 2004). The variability (scaled with u_*), ϕ_q and ϕ_c are also displayed on the *FluxPro* website. Interestingly, the close relationship between ϕ_θ and ε is shown in mid-subchart of Fig. 5, then more analysis will be represented at Subsection 3.2.

5) The *variation* chart (Fig. 6) presents the mean diurnal variation of lE and H over one week. The closed circles and light blue regions denote the weekly weighted mean trends and its 1σ on the basis of Equation (8) and (10), respectively, over the weeklong period (in the equations, J is set to 7). The circles and their whiskers denote an arithmetic mean and its 1σ, respectively. The vertical bars at the bottom of the subplots indicate the hourly acquisition ratios (ARs) over one week. The other type of variation chart displays the H and lE. Interestingly, the arithmetic mean of F is always smaller than the weighted mean at a given site. This result might be the clue of imbalance issue of EC measurement, because the weighted mean value generally exceeds the arithmetic mean.

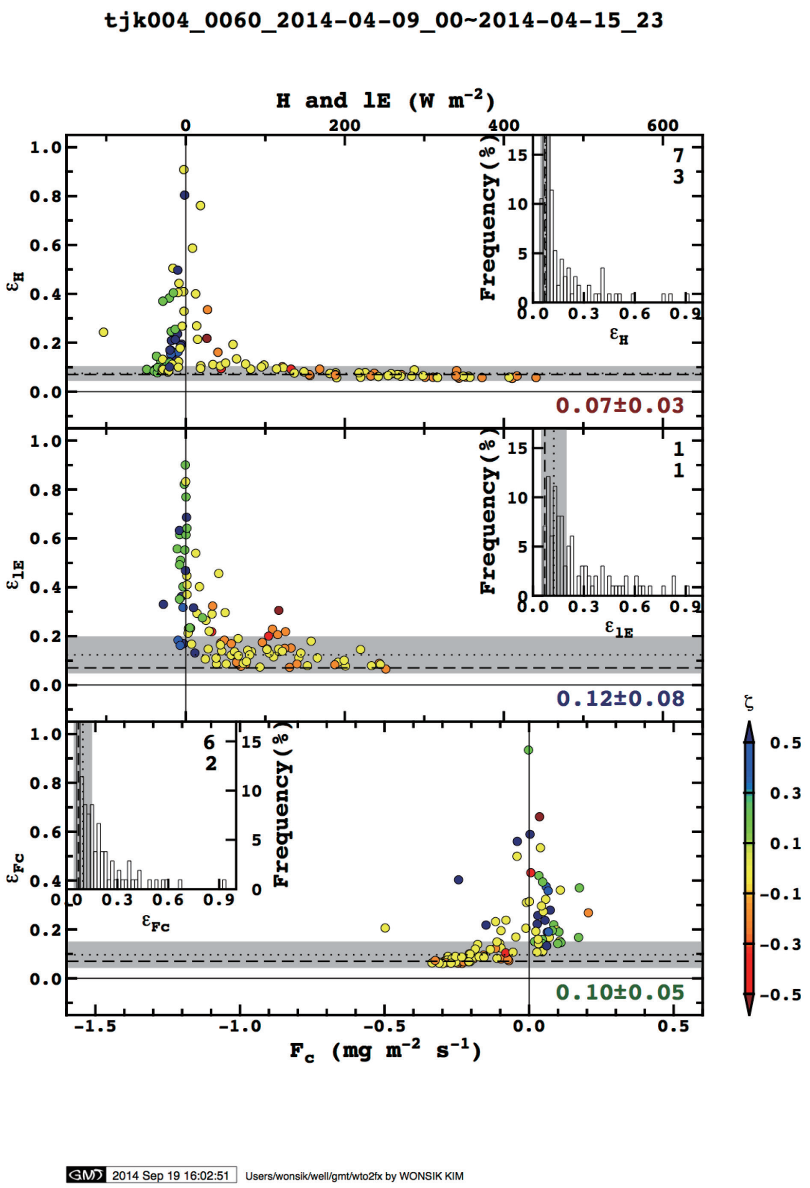

Fig. 3. The chart named *epsilon* in the *flux* cluster of *FluxPro*, showing the relationships between ε and F (scaled by ζ). Inserts show histograms of ε obtained from the dataset of Fig. 2. Details are given in 2) of Subsection 2.3.1.

2.3.2 The *raw*: analysis of turbulence time series

To facilitate identification of abnormal signals, the turbulence time series is presented in both the time and frequency domains under the *S system* tab *raw* on the *FluxPro* webpage (Table 2 and Figs. 7–8):

1) The *series* chart (Fig. 7) presents the auto- and cross-correlation functions (κ_{auto} and κ_{cross}; upper left and right subcharts) together with the turbulence time series of wind vectors and quantity scalars over one hour (plotted below the correlation subcharts). The κ determines the quality of the turbulence series on the basis of the atmospheric similarity and stationarity, and the time series of the spike corrections and trend analysis. In the autocorrelation plot, the purple, pink, orange, red, green and blue lines denote u, v, w, T, ρ_c and ρ_w, respectively. The dark red, green and blue lines in the cross-correlation plot denote the κ_{cross} between w and T, ρ_c and ρ_w, respectively. The dashed lines are proportional to $e^{-\sqrt{t/\pi}}$, denoting the κ under ideal turbulent conditions according to the the ergodic and Taylor's hypothesis. If the calculated κ_{cross} approaches this line, the turbulence exhibits high stationarity, and the F estimated from the turbulence measurement is of higher quality, even though it is just empirical line so far.

The midline in each of the series subcharts indicates the mean μ of the hourly data (the value is indicated parallel to the y-axis at the opposite side of the range indicator). The μ and their associated σ are also printed at the bottom of the charts, along with the total numbers of detected spikes and their ratios. The error and sigma spikes are defined at no data and over $\pm 5\sigma$ from μ, respectively. Spikes are indicated by black arrows on the time series charts.

The five-digit numbers following the tabulated results are the

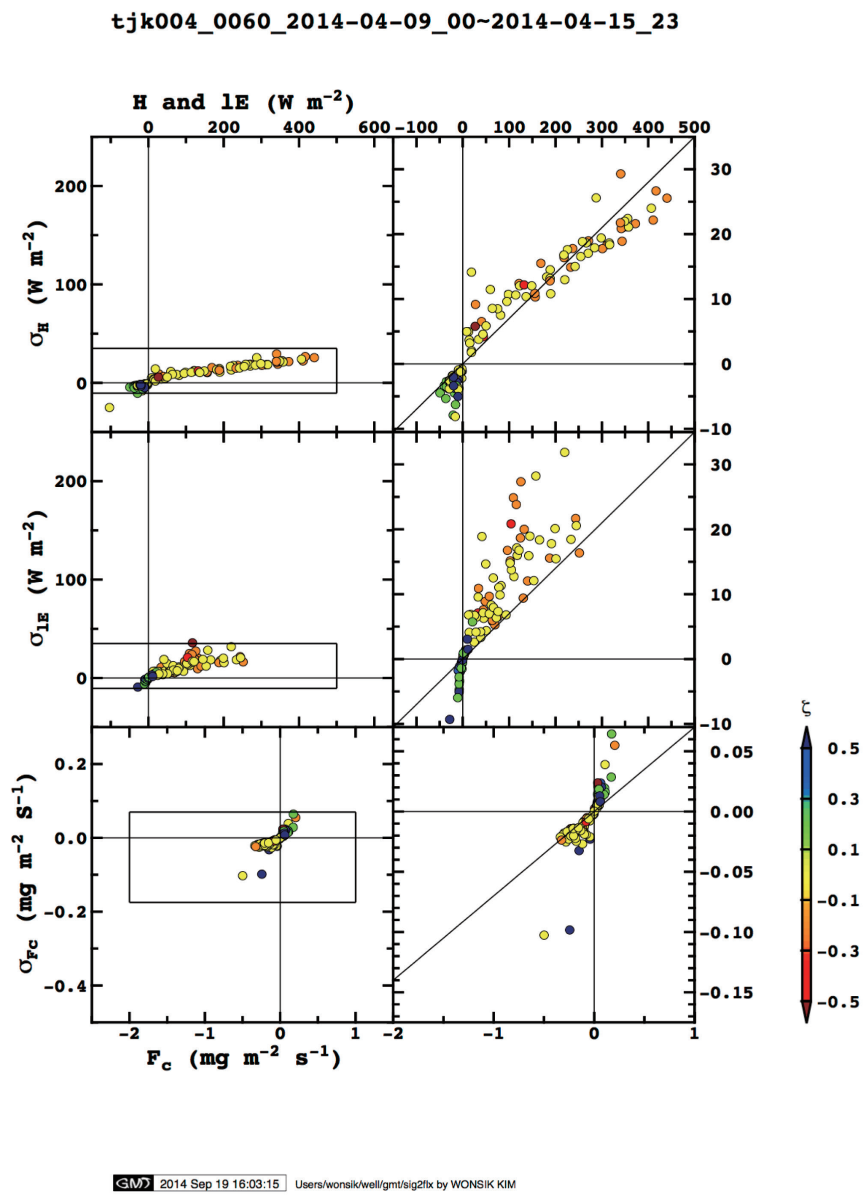

Fig. 4. The chart named *sigma* in the *flux* cluster of *FluxPro*, showing the relationship between σ and F (scaled by ζ) derived from the data set of Fig. 2. Details are given in 3) of Subsection 2.3.1.

time tags, indicating the day of year (three digits) and the hour of day (two digits). These are followed by the H, lE and F_c with those ε, the ϕ of T, ρ_c and ρ_w, the r between w and T, ρ_c and ρ_w, and instationarity (is) calculated in that order. The W_d, ζ and u_* are expressed as W_d, *as* and *us*, respectively (refer to Section 2.2.3).

2) The upper-left subchart of the *spectrum* chart (Fig. 8) presents normalized spectra of the wind vectors ($fS_\alpha(f)/\sigma_\alpha^2$, where f and S(f) are the frequency and spectral densities, respectively, and the subscript α denotes u, v, and w). The upper-right subchart displays the scalar quantities ($fS_\xi(f)/\sigma_\xi^2$, where ξ is T, ρ_c, and ρ_w), and the normalized cospectra ($fS_{w\xi}(f)/\overline{w'\xi'}$ are plotted at the lower left. The $S(f)$ is calculated by issuing the *spectrum1d* command in GMT, with the ensemble size and spacing set to 1024 and 0.1, respectively. The line in each subchart displays the expected spectral slope of the spectra ($f^{-2/3}$) and cospectra ($f^{-4/3}$), by which users can check the spectral similarity within an inertial subrange of turbulence measurements. The lower-right plot is the coherence ($Coh_{w\xi}^2$), which presents the r relative to f. This quantity is also calculated by *spectrum1d* under the same spectral conditions. The line colors are interpreted as described in Fig. 7. The theoretical background and the relationships between the spectral analysis and atmospheric turbulence are detailed in Chapter 8 and 9 in Stull (1988) and Chapter 2 and 3 in Kaimal and Finnigan (1994)

2.3.3 The *meteo*: the *V* to support *F* analysis

When considering environmental effects in the F analysis, it is useful to display the V variables. These variables are displayed as four charts under the *S system* tab *metro* on the *FluxPro* webpage (Table 2 and Figs. 9–12): 1) The *radiation* chart (Fig. 9) plots the radiation components, (*i.e.* the upward and downward short- and long-wave components, denoted as $R_{s,up}$, $R_{s,down}$, $R_{l,up}$ and

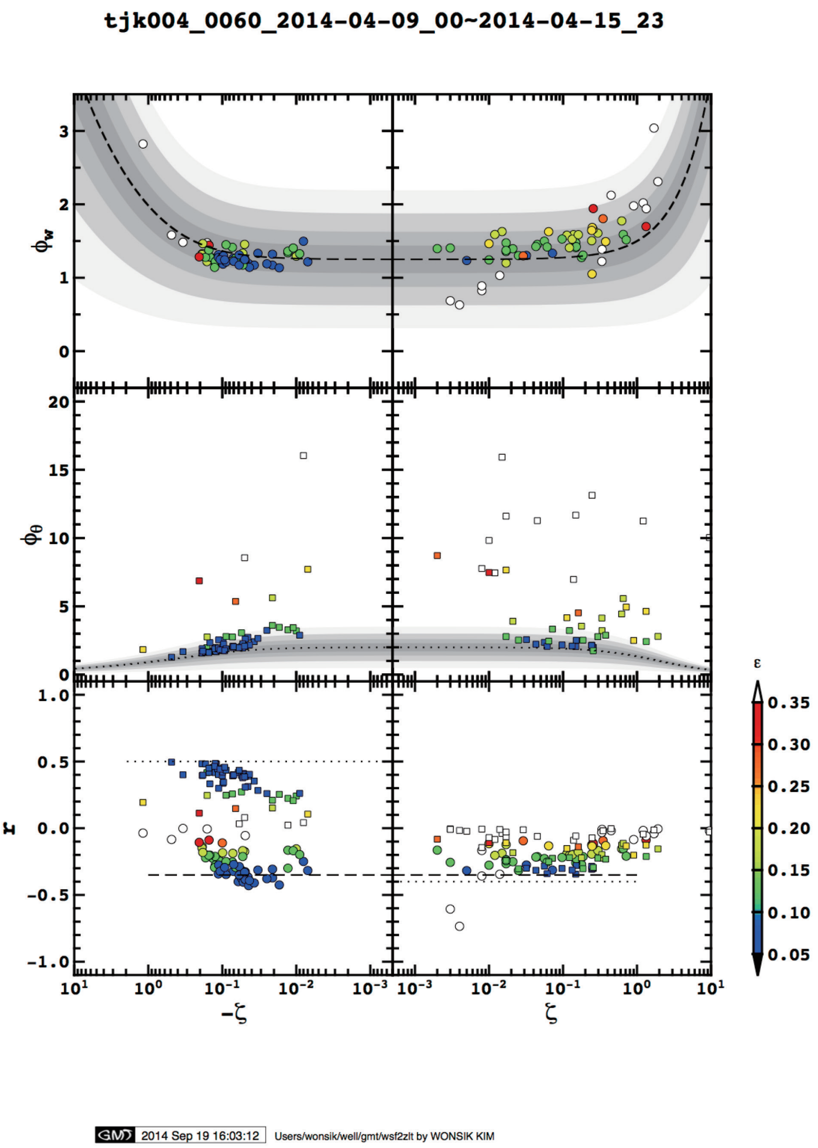

Fig. 5. One of the *variability* charts in the *flux* cluster of *FluxPro*, showing the relationships between ϕ (top and center) and r (bottom) and ζ (scaled by ε). The chart was derived from the data set of Fig. 2. Details are given in 4) of Subsection 2.3.1.

$R_{l,down}$, respectively), the net radiation R_n and the photosynthetic active radiation PAR over one week.

2) The *meteorology* chart (Fig. 10) plots the air and canopy temperatures (T_a and T_c, respectively), the relative humidity (RH), wind speed and wind direction (W_s and W_d, respectively), the precipitation (P), and the vapor pressure (e) throughout the same week.

3) The *EC* chart (Fig. 11) provides additional T_a, W_s, ρ_w, and ρ_c information, along with their $\pm\sigma$ measured by turbulence sensors. From these data, users can extract the background conditions at the EC site of interest.

4) The *windrose* chart (Fig. 12) presents the results of the W_d and W_s analyses as windroses and histograms. The green windrose is weighted by W_s. In both windroses, W_d is divided by 10°, and the magnitudes are normalized with respect to the most frequent W_d, which is set to 1.0.

2.3.4 The *annual*: seasonal and inter-annual analysis of *F*

To assess the seasonal and inter-annual variability of F, the user can display the hourly and monthly F throughout one year under the *S system* tabs *annual* on the *FluxPro* webpage (Table 2 and Figs. 13–14):

1) The *trend* chart (Fig. 13) presents the monthly and hourly trends in H, lE, and F_c over one year. The top subchart displays the integrated values of H (dark red), evapotranspiration ET (dark blue) and net ecosystem exchange NEE (dark green) throughout the year, together with their uncertainties. In the hour ly display, F is scaled by ε and the numerals at the top-left and top-right of the subcharts state the uncertainties and acquisition ratios, respectively, during the analyzed year.

2) The *contour* chart (Fig. 14) displays hourly contours of H and lE throughout one year. This is useful if a user desires to know the daily and monthly variability of these parameters. The F_c contour chart is also visible at *FluxPro* webpage (the chart is not shown here).

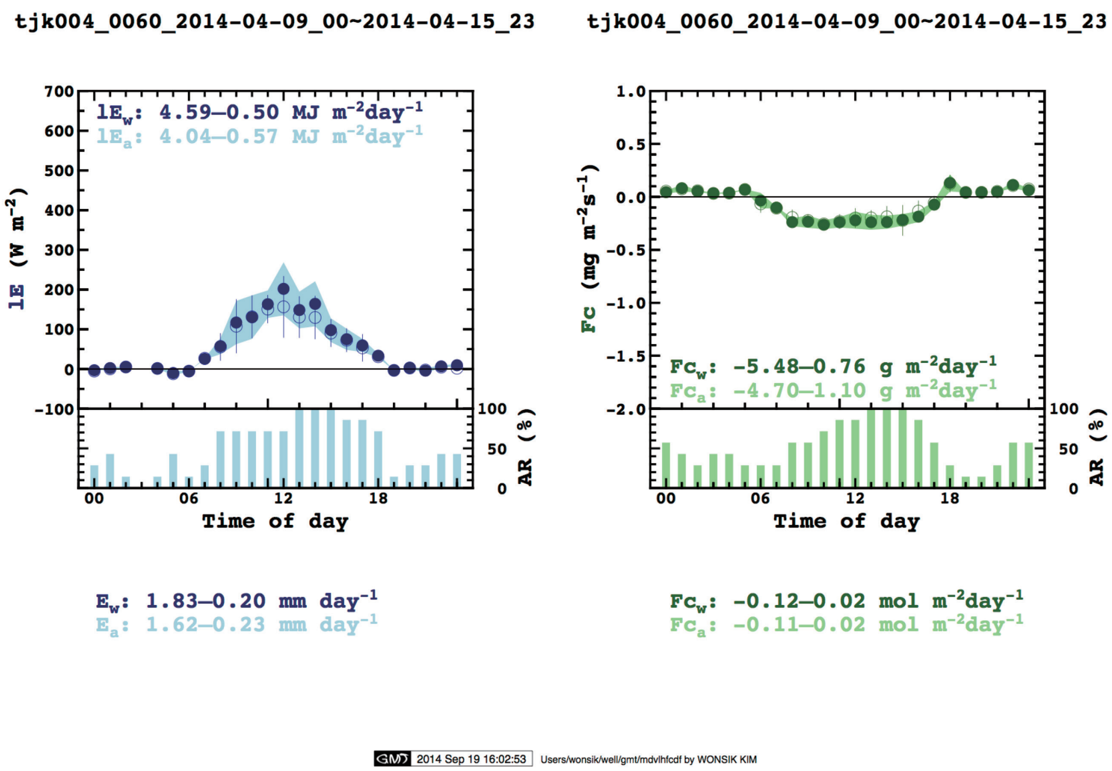

Fig. 6. One of the *variation* charts in the *flux* cluster of *FluxPro*, showing the mean diurnal variation of lE and F_c derived from the dataset of Fig. 2. Details are given in 5) of Subsection 2.3.1.

3. Results and Discussion

This section presents specific results of the *FluxPro* processing and ε analysis of EC measurements, and discusses their importance. The data policy of *FluxPro* is also presented for readers who are interested in our EC measurements and *FluxPro* code.

3.1 General

Since its launch in 2009, *FluxPro* has been subject to ongoing systems development and continuous site participation, EC measurements from 16 sites in Asia can now be accessed at the *AgroMeteorological Nowcaster* website links http://matthew.niaes.affrc.go.jp/amen/top/top.htm and http://matthew.niaes.affrc.go.jp/amen/sites/sites.htm. *FluxPro* has become a basic system for the *AgroMeteorological Nowcaster* (http: //matthew.niaes.affrc.go.jp/amen/) enabling evapotranspiration and net ecosystem exchange estimates at any spatiotemporal scale. The top of the Nowcaster homepage features two tabs, *FluxPro* and *sFluxPro*. The first is linked to a full version of the *FluxPro* webiste presenting data from the entire 16 sites in the form of various useful charts (Subsection 2.3). The *sFluxPro* links to a simpler version of *FluxPro*, presenting 10 sites in the form of weeks and variation charts (http://matthew.niaes.affrc.go.jp/amen/simple/simple.htm). The *sFluxPro* allows access to realtime measurements from ten sites, enabling a quick check for site management and maintenance, whereas *FluxPro* allows access to an additional six sites where the measurements are manually acquired because telecommunication devices and/or financial support sources are lacking.

Any investigator interested in measurements at each individual site can access the measurements and information provided by *FluxPro*, not only for his or her own site but also for sites managed by others participating in *FluxPro*. Visitors can also scrutinize the *FluxPro* measurements to enhance understanding in their own fields. Specifically, an investigator managing his own site can view *FluxPro*-generated charts online and can receive automatic email alerts, circumventing the need to undertake troublesome instrumental or administrative procedures to manage and maintain his own remote site. Moreover, any investigator or visitor can download *FluxPro* measurements of special interest, and use them in their own scientific quests while investing minimal effort in site management, measurement inspection, and chart presentation. Charts comparing measurements at different sites are also available for comparative purposes. Figure 15 is an example of a chart obtained from the AgroMeteorological Nowcaster website (http://matthew.niaes.affrc.go.jp/amen/top/top.htm). This information is particularly useful to colleagues undertaking an integration or consolidation analysis of realtime measurements acquired at various sites.

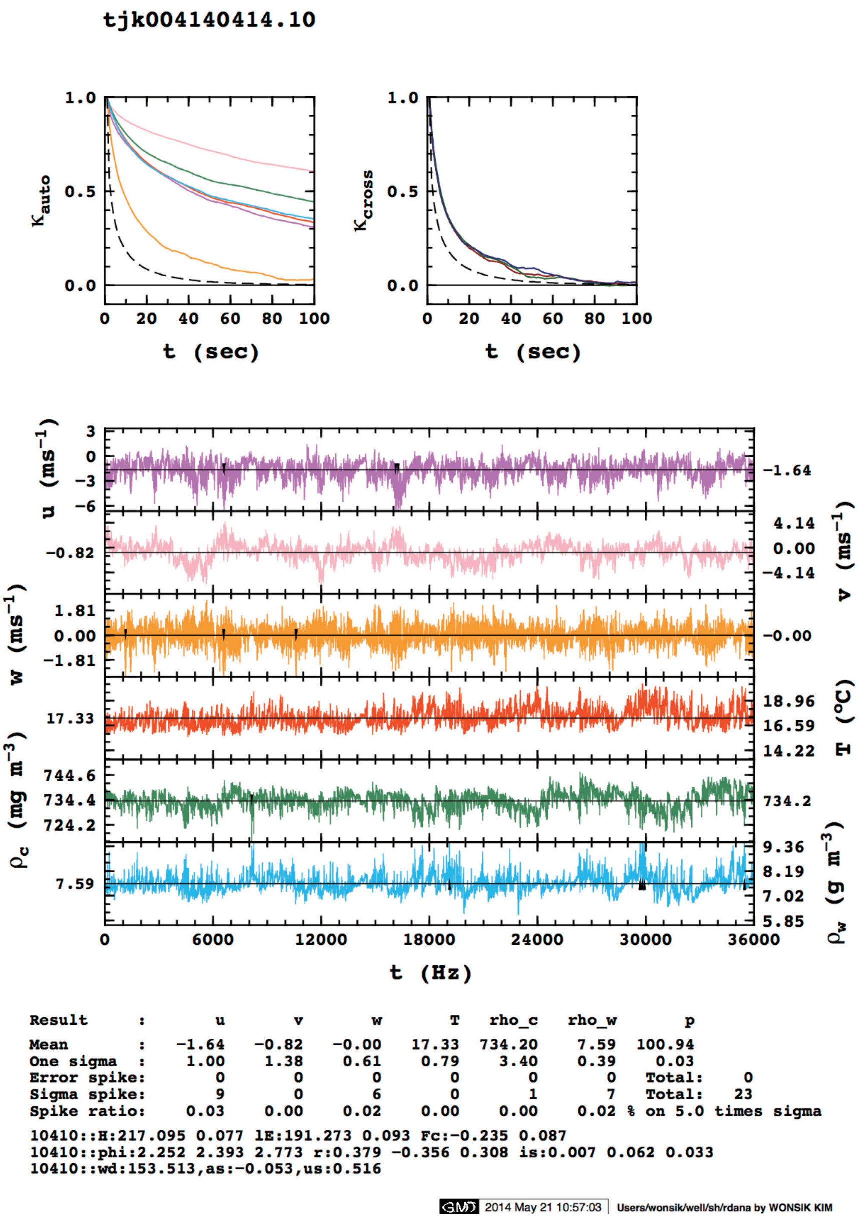

Fig. 7. One of the *series* charts in the *raw* cluster of *FluxPro*, showing the raw data analysis of turbulence measurements taken from 10:00:00 0 Hz to 10:59:59 9 Hz on 14 April, 2014 at a tangerine orchard in Jeju, Korea. Details are given in 1) of Subsection 2.3.2.

Inspection of EC measurements is necessary for assessing the reliability of the measurements. A traditional inspection involves a stationary test, an integral turbulence test, and footprint analysis (Foken *et al.*, 2004). The inspection reveals whether measurements obtained under real environmental conditions approach the theoretical assumptions underlying empirical criteria. The ε parameter adopted by *FluxPro* (Figs. 3, 2) is based on the statistical background and rare empirical criteria (Fuller, 1996; Bendat and Piersol, 2000; Finkelstein and Sims, 2001) in routine QCQA and uncertainty analysis, as well as on traditional considerations. Time trends (Fig. 7) and spectra and cospectra (Fig. 8) of turbulence processed on an hourly basis ensure consistent and reliable F estimation. Therefore, it is possible to consider that the inspection produced by *FluxPro* could be profitable for various EC measurements using diverse sonic anemometers and gas analyzers under suitable corrections applying to *FluxPro* for the instruments.

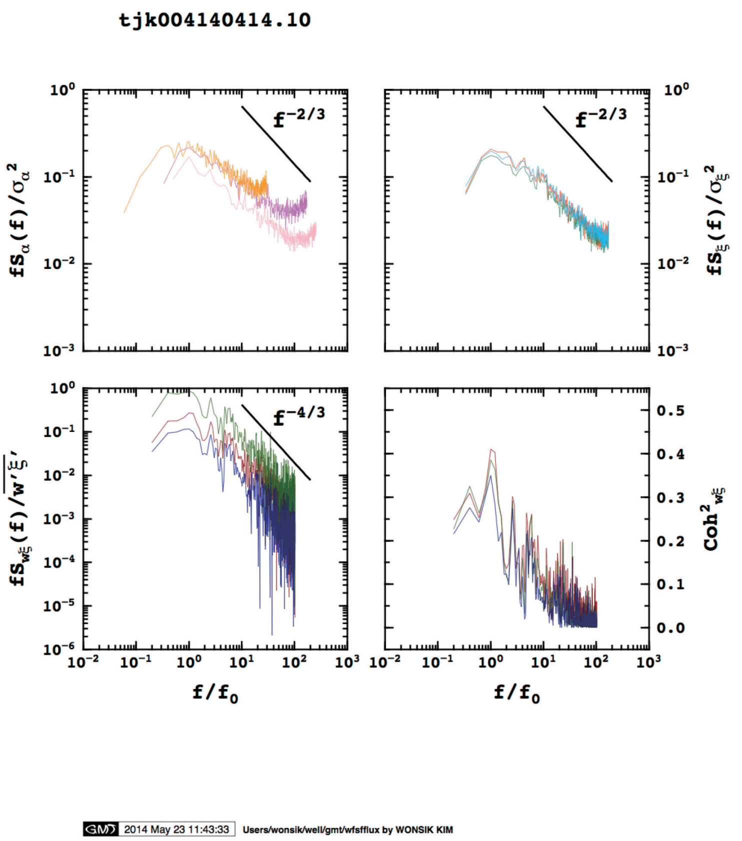

Fig. 8. One of the *spectra* charts in the *raw* cluster of *FluxPro*, showing the spectral analysis of the data in Fig. 7. Details are given in 2) of Subsection 2.3.2.

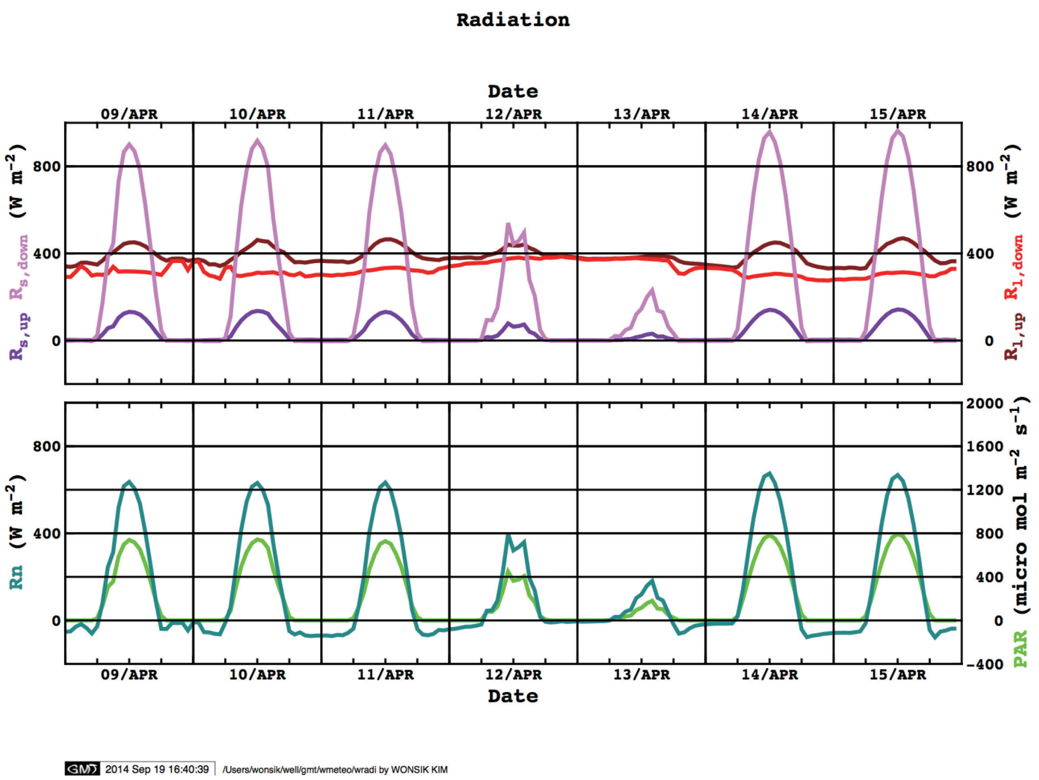

Fig. 9. The *radiation* chart in the *metro* cluster of *FluxPro*, showing the diurnal cycle of the radiation components from 00:00:00 on 9 April to 23:50:00 on 15 April, 2014, at a tangerine orchard in Jeju, Korea. Details are given in 1) of Subsection 2.3.3.

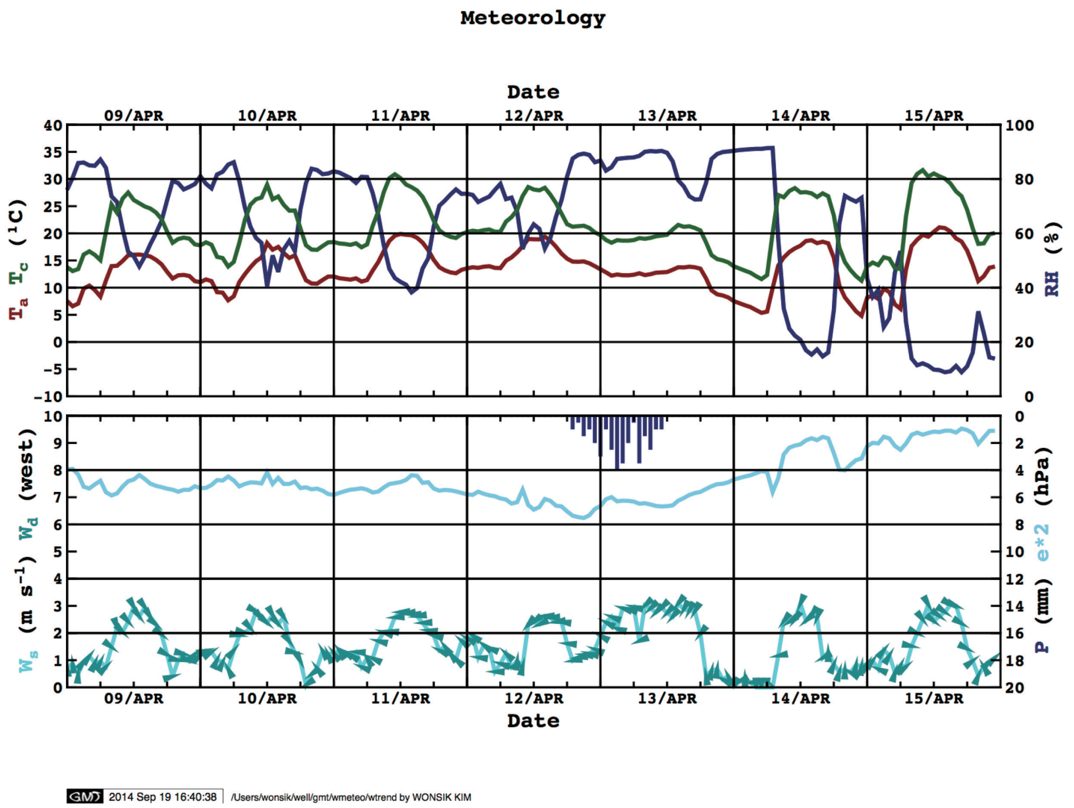

Fig. 10. The *meteorology* chart in the *metro* cluster of *FluxPro*, showing the diurnal cycle of the meteorological components over the period specified in Fig. 9. Details are given in 2) of Subsection 2.3.3.

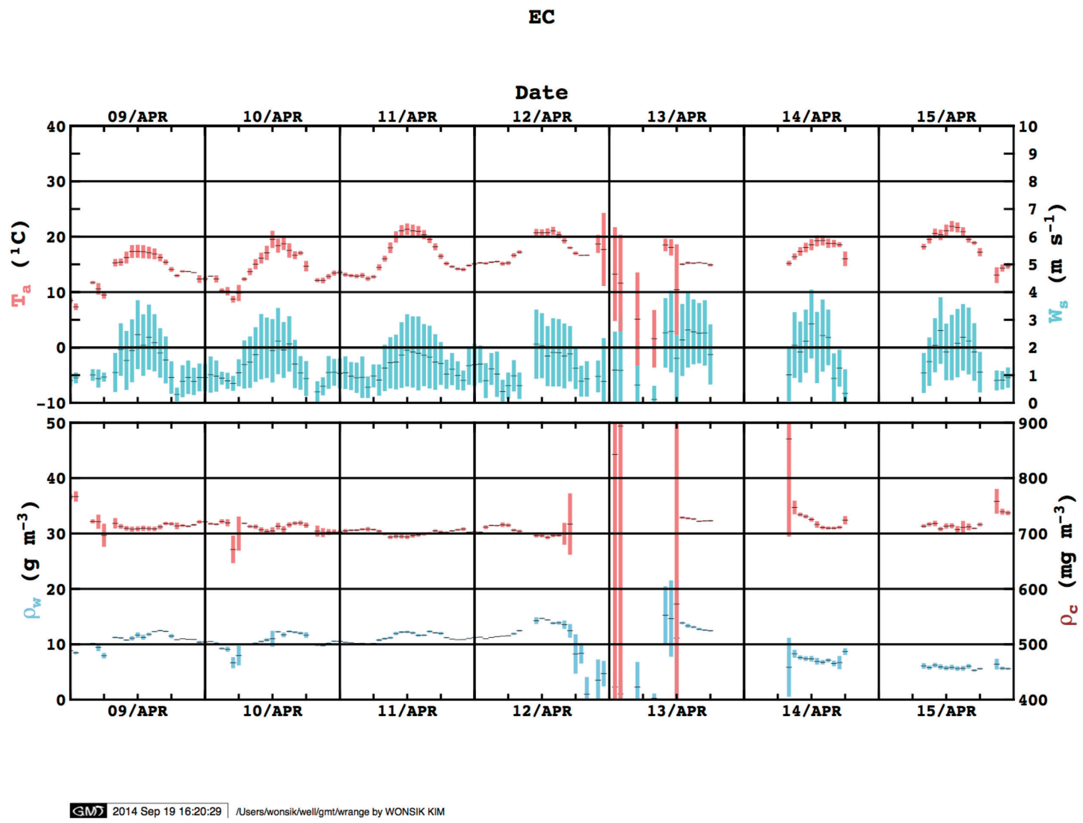

Fig. 11. The *ec* chart in the *metro* cluster of *FluxPro*, showing the diurnal cycle of $\mu \pm \sigma$ derived from the dataset of Fig. 2. Details are given in 3) of Subsection 2.3.3.

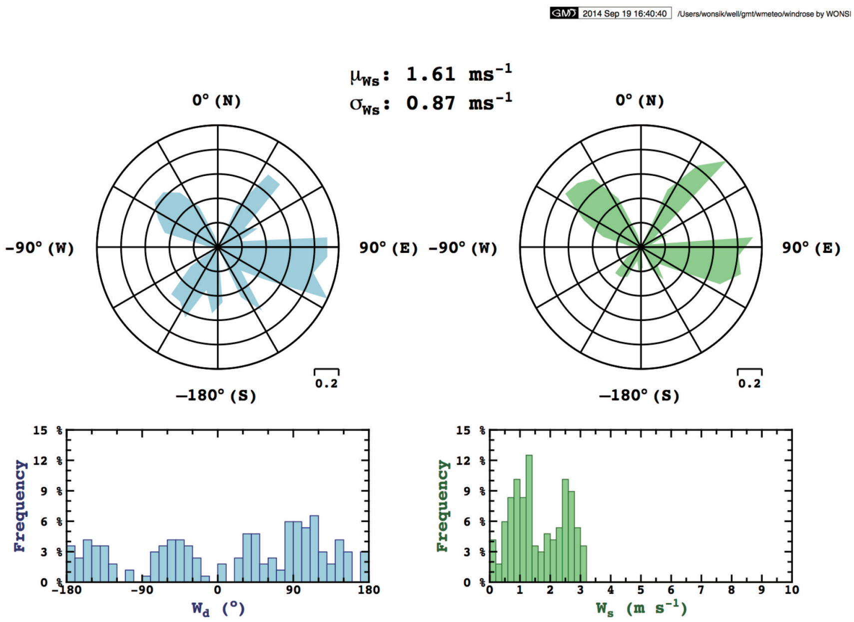

Fig. 12. The *windrose* chart in the *metro* cluster of *FluxPro*, showing the windroses (top) and histograms (bottom) of W_d and W_s data over the period specified in Fig. 9. Details are given in 4) of Subsection 2.3.3.

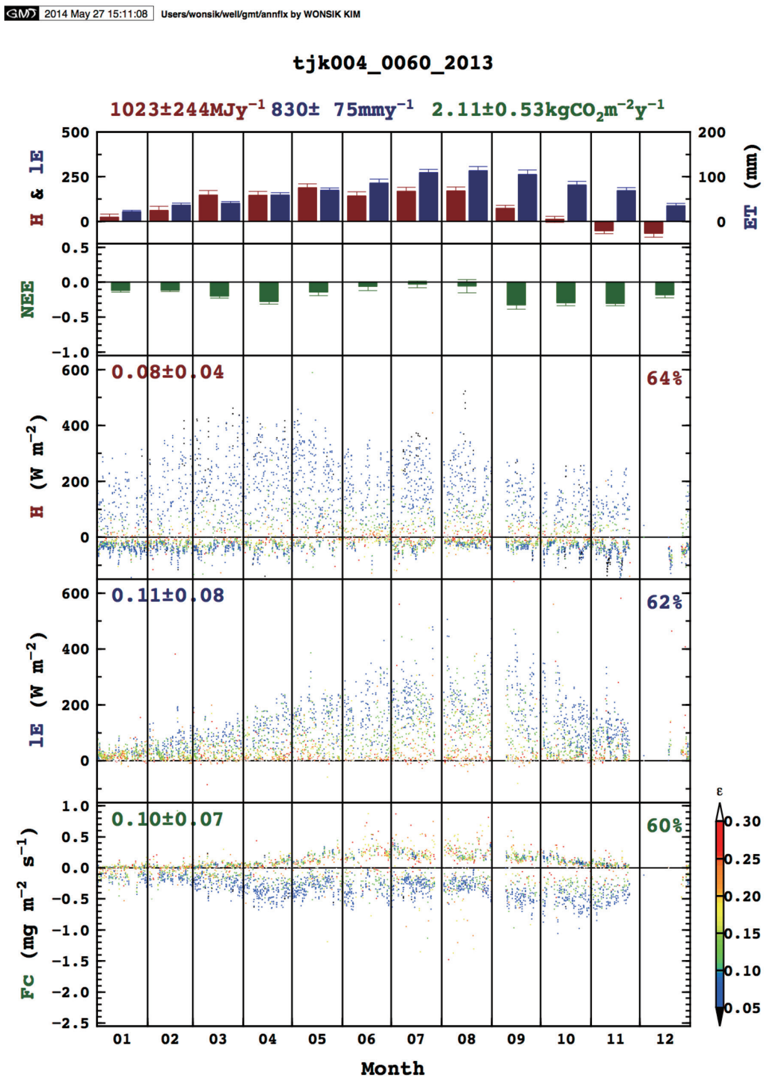

Fig. 13. The *trend* chart in the *annual* cluster of *FluxPro*, showing the monthly and hourly *F* trends throughout 2013 in a cassava field at Tak, Thailand. Details are given 1) of Subsection 2.3.4.

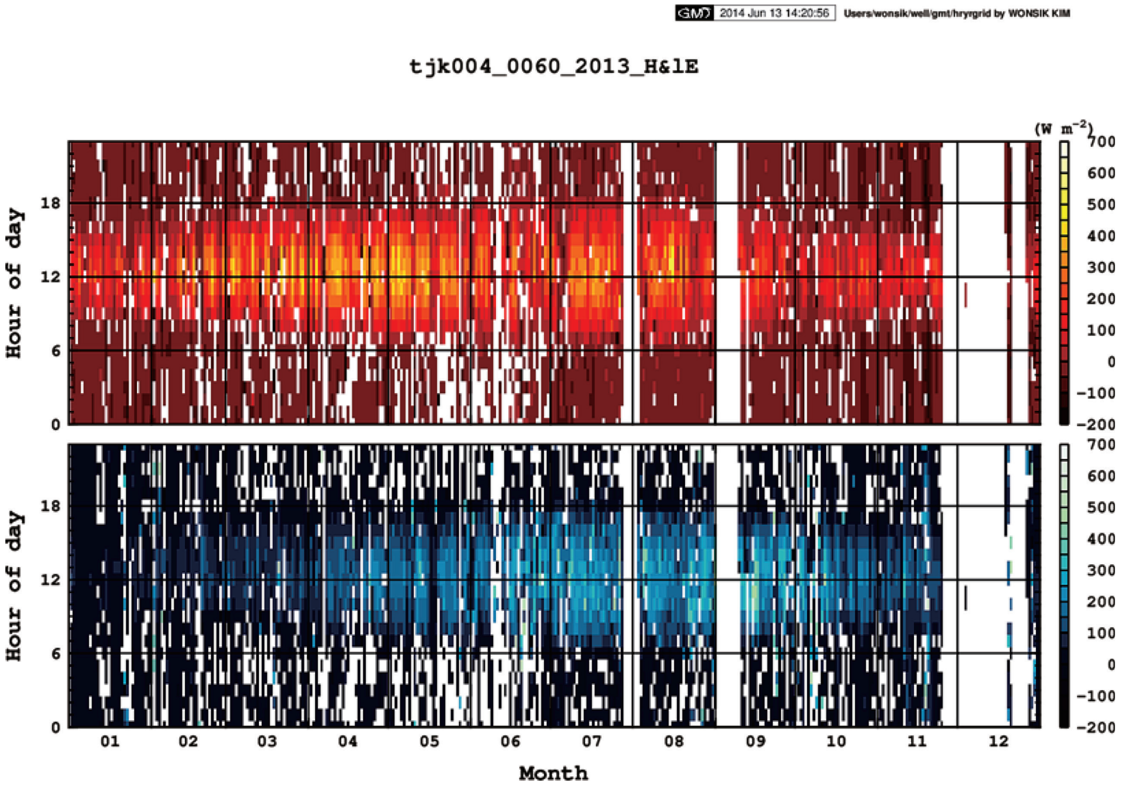

Fig. 14. One of the *contour* charts in the *annual* cluster of *FluxPro*, showing the variation in *H* and *lE* derived from the dataset of Fig. 13. Details are given in 2) of Subsection 2.3.4.

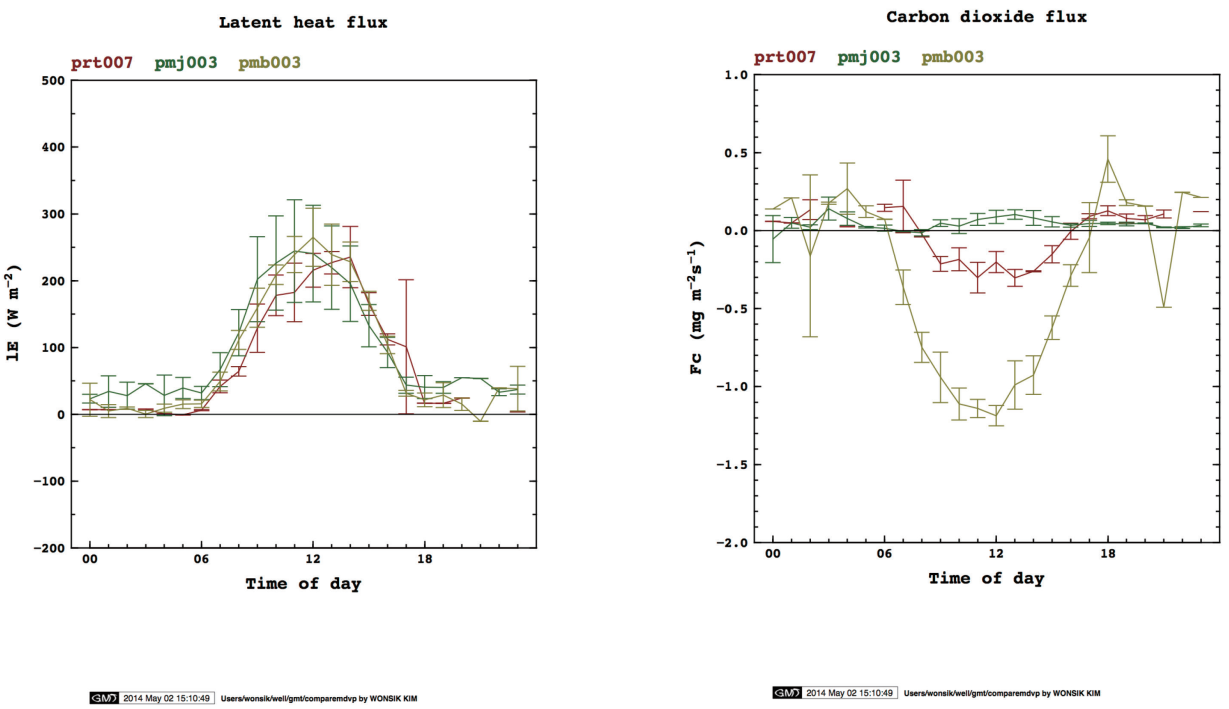

Fig. 15. Sample charts comparing of the mean diurnal variation of *lE* and F_c from 09:00 on 18 March to 08:59 on 24 March, 2014. Data were collected form a paddy field in Rachaburi, Thailand (prt007), Mase in Japan (pmj003) and Mymensingh in Bangladesh (pmb003).

Finally, the covariance of turbulences enables temporary *F* estimation by the data logger itself. However, this option is not recommended because the calculation consumes significant CPU time; consequently, regular gaps may appear in the turbulence data. In addition, the procedure may yield an irregular integer output rather than a real number, and the effect on the turbulence spectrum may not be clarified. Therefore, a data logger exclusively devoted to recording the turbulence data should be installed to avoid measurement gaps.

3.2 Uncertainty in the *FluxPro* estimates

Any measured physical quantity representing some property of an object contains uncertainty introduced by inherent flaws in the measuring instrument. In other words, the inaccuracy of a measured quantity reflects the quality of the measurement. The uncertainty of measured value specifies an interval within which the true value lies with a given probability (Rabinovich, 2005). Therefore, knowing the uncertainty can be equally or perhaps more important than knowing the value itself. For this reason, *FluxPro* provides both the values and uncertainties of hourly F estimates. The Fs are then averaged or integrated over weekly, monthly and yearly timeframes by propagating the hourly uncertainty as described in Subsection 2.2.2. The resulting ε value is about 10%–30% (minimum about 5%–7%) over the entire set for investigative sites in *FluxPro*. The information could be easily compared with F estimated by numerical models or satellite analysis based on statistical significance.

Atmospheric turbulence characterizes a similarity, and has a specific function of ζ. Therefore, this function has been traditionally used for QCQA of EC measurement. Comparing ε and ϕ (Figs. 16, 5), we observe that ε could provide an alternative scaling parameter for QCQA of EC measurements. In fact, ε might prove more useful than ϕ because it contains information of statistical uncertainty in the EC measurements. As shown in Fig. 16, the minimum uncertainty in the EC measurements is approximately 7% under neutral conditions, because the y intercept of ε is $\simeq$0.07 when ϕ = 2 where F is measured under ideally turbulence conditions. This result suggests that every EC measurement includes 7% uncertainty under neutral conditions; moreover, it sug-

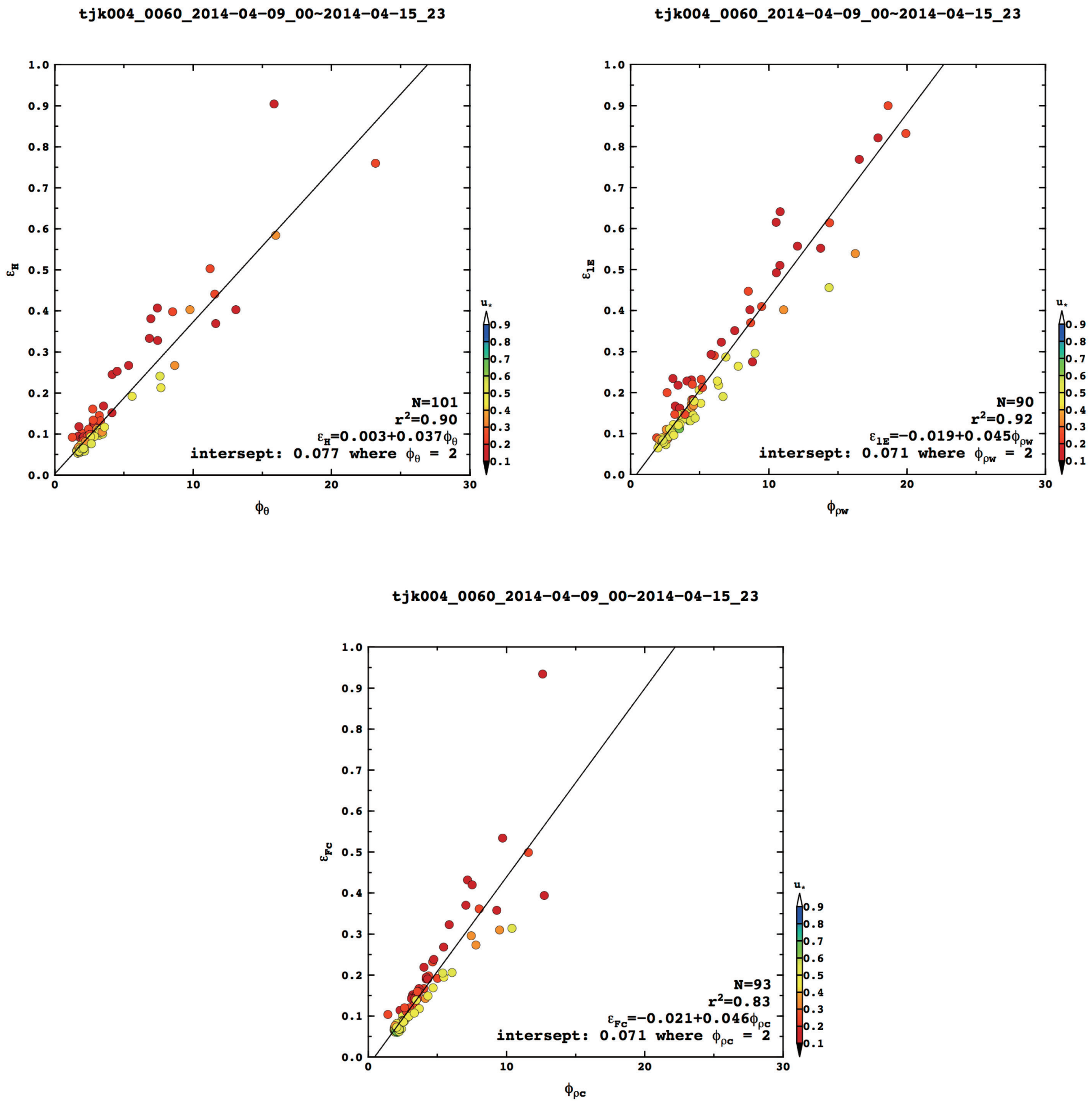

Fig. 16. Relationship between ε and ϕ based on the dataset of Fig. 2.

gests that the uncertainty is a function of ζ; even though this contrasts with previous studies (Kim *et al*., 2008, 2009, 2011a,b), in which the minimum uncertainty was regarded as constant.

Lastly, uncertainty information contains not only the inherent inaccuracy in F but also the effective heterogeneity η in the EC measurements. This hypothesis, suggested by Kim *et al*. (2011b) and Kim *et al*. (2014), implies that η requires evaluation over a spatial distribution of F.

3.3 Data policy

The basic philosophy of *FluxPro* is to encourage data sharing. Every EC measurement integrated by *FluxPro* is available to any parties interested in our measurements, providing that they honor the site investigators engaged in flux observations. Every member of the *FluxPro* committee believes that every measurement collected by colleagues around the globe is a very valuable scientific resource, and that the ethical use and publication of measurements is the right and duty of everyone. Therefore, *FluxPro* sincerely encourages colleagues to access the *FluxPro* measurements, and report their interpretations and analyses in appropriate scientific publications. During contemplation and analysis, *FluxPro* allows users to inform each PI of flux measurement sites, and acknowledges or offers author participation when a manuscript is submitted for publication. A few sites are excluded from direct downloads of measurements from the *FluxPro* website. Nevertheless, visitors can access the measurements suitable for their own scientific projects with the consideration and permission of the site PI. Finally, *FluxPro* code can be requested via an email (wonsik@affrc.go.jp) on the basis of GNU philosophy.

4. Conclusions

We conclude this paper by summarizing the benefits of *FluxPro*.

1) *FluxPro* monitors the flux density (F), its uncertainty (ε), and several affiliated micrometeorological variables (V) in an internet webpage in realtime. Surveilling these measurements, *FluxPro* also manages multiple eddy covariance (EC) flux measurement sites with features that conveniently deal with F computation and promptly cope with management disturbances.

2) *FluxPro* comprises a gathering system, which acquires EC measurements from each site and relays them to the *FluxPro* management server; a cooking system that computes F, ε and V; and a serving system that presents *FluxPro* results online and in an accessible format for colleagues in several disciplines.

3) *FluxPro* is designed to estimate ε of F, which is essential for quality control and quality assurance, to estimate land surface heterogeneity, and to weight the averaged and integrated F estimate. The ε might be one of the parameters of Monin-Obukhov similarity.

4) *FluxPro* database storing the computed F and V and the primary turbulence measurement is freely available for investigation by interested parties via internet download and email request.

Acknowledgments

This study was partially supported by the Science and Technology Research Partnership for Sustainable Development, Japan Science and Technology Agency/Japan International Cooperation Agency, and the Asia-Pacific Network for Global Change Research (ARCP2014-04CMY-Miyata).

References

Baldocchi, D., Falge, E., Gu, L., Olson, R., Hollinger, D., Running, S., Anthoni, P., Bernhofer, C., Davis, K., Evans, R., Fuentes, J., Goldstein, A., Katul, G., Law, B., Lee, X., Malhi, Y., Meyers, T., Munger, W., Oechel, W., PawU, K. T., Pilegaard, K., Schmid, H. P., Valentini, R., Verma, S., Vesala, T., Wilson, K., and Wofsy, S., 2001: Fluxnet: A new tool to study the temporal and spatial variability of ecosystem-scale carbon dioxide, water vapor, and energy flux densities. *Bulletin of the American Meteorological Society*, **82**, 2415–2434.

Bendat, J. S., and Piersol, A. G., 2000: *Random Data: Analysis and Measurement Procedures*. (3rd ed.). John Wiley and Sons.

Burba, G. G., Mcdermitt, D. K., Grelle, A., Anderson, D. J., and Xu, L., 2008: Addressing the influence of instrument surface heat exchange on the measurements of CO_2 flux from open-path gas analyzers. *Global Change Biology*, **14**, 1854–1876.

Falge, E., Baldocchi, D., Olson, R., Anthoni, P., Aubinet, M., Bernhofer, C., Burba, G., Ceulemans, R., Clement, R., Dolman, H., Granier, A., Gross, P., Grünwald, T., Hollinger, D., Jensen, N.-O., Katul, G., Keronen, P., Kowalski, A., Lai, C. T., Law, B. E., Meyers, T., Moncrieff, J., Moors, E., Munger, J. W., Pilegaard, K., Rannik, Ü, Rebmann, C., Suyker, A., Tenhunen, J., Tu, K., Verma, S., Vesala, T., Wilson, K., and Wofsy, S., 2001: Gap filling strategies for defensible annual sums of net ecosystem exchange. *Agricultural and Forest Meteorology*, **107**, 43–69.

Finkelstein, P., and Sims, P., 2001: Sampling error in eddy correlation flux measurements. *Journal of Geophysical Research*, **106**, 3503–3509.

Finnigan, J. J., 2004: A re-evaluation of long-term flux measurement techniques part ii: Coordinate systems. *Boundary-Layer Meteorology*, **113**, 1–41.

Finnigan, J. J., Clement, R., Malhi, Y., Leuning, R., and Cleugh, H. A., 2003: A re-evaluation of long-term flux measurement techniques part i: Averaging and coordinate rotation. *Boundary-Layer Meteorology*, **107**, 1–48.

Foken, T., Göcede, M., Mauder, M., Mahrt, L., Amiro, B., and Munger, W., 2004: Post-field data quality control. In X. Lee, W. Massman, and B. Law (Eds.), *Handbook of Micrometeorology* (pp. 181–208). Kluwer Academic Publishers, The Netherlands.

Foken, T., and Wichura, B., 1996: Tools for quality assessment of surface-based flux measurements. *Agricultural and Forest Meteorology*, **78**, 83–105.

Fuller, W. A., 1996: *Introduction to Statistical Time Series*. (2nd ed.). John Wiley and Sons.

Hollinger, D. Y., and Richardson, A. D., 2005: Uncertainty in eddy covariance measurements and its application to physiological models. *Tree Physiology*, **25**, 873–885.

Jung, M., Reichstein, M., Margolis, H. A., Cescatti, A., Richardson, A. D., Arain, M. A., Arneth, A., Bernhofer, C., Bonal, D., Chen, J., Gianelle, D., Gobron, N., Kiely, G., Kutsch, W., Lasslop, G., Law, B. E., Lindroth, A., Merbold, L., Montagnani, L., Moors, E. J., Papale, D., Sottocornola, M., and Williams, F. V. C., 2011: Global patterns of land-atmosphere fluxes of carbon dioxide, latent heat, and sensible heat derived from eddy covariance, satellite, and meteorological observations. *Journal of Geophysical Research*, **116**, G00J07.

Kaimal, J. C., and Finnigan, J. J., 1994: *Atmospheric Boundary Layer Flows: Their Structure and Measurement*. Oxford University Press.

Kaimal, J. C., and Gaynor, J. E., 1991: Another look at sonic thermometry. *Boundary-Layer Meteorology*, **56**, 401–410.

Kato, T., Knorr, W., Scholze, M., Veenendaal, E., Kaminski, T., Kattge, J., and Gobron, N., 2013: Simultaneous assimilation of satellite and eddy covariance data for improving terrestrial water and carbon simulations at a semi-arid woodland site in Botswana. *Biogeosciences*, **10**, 789–802.

Kim, W., Cho, J., Komori, D., Aoki, M., Yokozawa, M., Kanae, S., and Oki, T., 2011a: Tolerance of eddy covariance flux measurement. *Hydrological Research Letters*, **5**, 73–77.

Kim, W., Cho, J., Myong, G., Mano, M., Komori, D., and Kim, S. D., 2008: Quality assessment of data from the Daegwallyeong flux measurement station (DFMS) based on short-term experiments. *Journal of Agricultural Meteorology*, **64**, 111–120.

Kim, W., Kim, H., Kim, J., Agata, Y., Miyazaki, S., and Oki, T., 2003: Real time monitoring and simulation system (RTMASS) for Tak flux measurement site, Thailand. *Korean Journal of Agricultural and Forest Meteorology*, **5**, 116–127.

Kim, W., Komori, D., and Cho, J., 2009: The characteristic of relative error in eddy covariance measurements and its application to data quality control in rainfed paddy field. *Journal of Agricultural Meteorology*, **65**, 201–207.

Kim, W., Komori, D., and Cho, J., 2011b: The characteristic of fractional uncertainty on eddy covariance measurement. *Journal of Agricultural Meteorology*, **67**, 163–171.

Kim, W., Komori, D., Cho, J., Kanae, S., and Oki, T., 2014: Long-term analysis of evapotranspiration over diverse land use area in northern Thailand. *Hydrological Research Letters*, **8**, 45–50.

Kim, Y., Kimball, J. S., Zhang, K., and McDonald, K. C., 2012: Satellite detection of increasing northern hemisphere non-frozen seasons from 1979 to 2008: Implications for regional vegetation growth. *Remote Sensing of Environment*, **121**, 472–487.

Leuning, R., 2004: Measurements of trace gas fluxes in the atmosphere using eddy covariance: WPL corrections revisited. In X. Lee, W. Massman, and B. Law (Eds.), *Handbook of Micrometeorology* (pp.119–132). Kluwer Academic Publishers, The Netherlands.

Li, Z. L., Tang, R., Wan, Z., Bi, Y., Zhou, C., Tang, B., Yan, G., and Zhang, X., 2009: A review of current methodologies for regional evapotranspiration estimation from remotely sensed data. *Sensors*, **9**, 3801–3853.

Liu, H., Peters, G., and Foken, T., 2001: New equations for sonic temperature variance and buoyancy heat flux with an omnidirectional sonic anemometer. *Boundary-Layer Meteorology*, **100**, 459–468.

Lu, J., Sun, G., McNulty, S. G., and Amatya, D. M., 2005: A comparison of six potential evapotranspiration methods for regional use in the southeastern united states. *Journal of the American Water Resources Association*, **41**, 621–633.

Massman, W. J., and Clement, R., 2004: Uncertainty in eddy covariance flux estimates resulting from spectral attenuation. In X. Lee, W. Massman, and B. Law (Eds.), *Handbook of Micrometeorology* (pp.67–99). Kluwer Academic Publishers, The Netherlands.

Meyers, T. P., Finkelstein, P., Clarke, J., Ellestad, T. G., and Sims, P. F., 1998: A multilayer model for inferring dry deposition using standard meteorological measurements. *Journal of Geophysical Research*, **103**, 22645– 22661.

Moncrieff, J., Clement, R., Finnigan, J., and Meyers, T., 2004: Averaging, detrending, and filtering of eddy covariance time series. In X. Lee, W. Massman, and B. Law (Eds.), *Handbook of Micrometeorology* (pp.7– 31). Kluwer Academic Publishers, The Netherlands.

Rabinovich, S. G., 2005: *Measurement Errors and Uncertainties: theory and Practice*. Springer.

Sheffield, J., Wood, E. F., Chaney, N., Guan, K., Sadri, S., Yuan, X., Olang, L., Amani, A., Ali, A., Demuth, S., and Ogallo, L., 2014: A drought monitoring and forecasting system for sub-Sahara African water resources and food security. *Bulletin of the American Meteorological Society*, **95**, 861–882.

Stull, R. B., 1988: *An Introduction to Boundary Layer Meteorology*. Kluwer Academic Publishers.

Vickers, D., and Mahrt, L., 1997: Quality control and flux sampling problems for tower and aircraft data. *Journal of Atmospheric and Oceanic Technology*, **14**, 512–526.

Vickers, D., Thomas, C., and Law, B. E., 2009: Random and systematic CO_2 flux sampling errors for tower measurements over forests in the convective boundary layer. *Agricultural and Forest Meteorology*, **149**, 73–83.

Webb, E. K., Pearman, G. I., and Leuning, R., 1980: Correction of flux measurements for density effects due to heat and water vapour transfer. *The Quarterly Journal of the Royal Meteorological Society*, **106**, 85–100.

Willis, G. E., and Deardorff, J. W., 1976: On the use of Taylor's translation hypothesis for diffusion in the mixed layer. *The Quarterly Journal of the Royal Meteorological Society*, **102**, 817–822.